



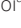






Upregulation of Robo4 expression by SMAD signaling suppresses vascular permeability and mortality in endotoxemia and COVID-19 models

Maaya Morita^a, Aki Yoneda^a, Nagisa Tokunoh^{b,c}, Tatsumi Masaki^a, Keisuke Shirakura^a , Mayumi Kinoshita^a, Rina Hashimoto^d , Naoya Shigesada^a, Junya Takahashi^a, Masashi Tachibana^a , Shota Tanaka^a, Masanori Obana^{a,e}, Nobumasa Hino^a, Masahito Ikawa^{a,b,e} , Kazutake Tsujikawa^a, Chikako Ono^{b,e}, Yoshiharu Matsuura^{b,e}, Hiroyasu Kidoya^f, Nobuyuki Takakura^{b,e}, Yoshiaki Kubota^g , Takefumi Doi^a, Kazuo Takayama^d , Yasuo Yoshioka^{a,b,c,e}, Yasushi Fujio^{a,e}, and Yoshiaki Okada^{a,e,1} 

Edited by Napoleone Ferrara, University of California San Diego, La Jolla, CA; received August 10, 2022; accepted December 7, 2022

There is an urgent need to develop novel drugs to reduce the mortality from severe infectious diseases with the emergence of new pathogens, including Coronavirus disease 2019 (COVID-19). Although current drugs effectively suppress the proliferation of pathogens, immune cell activation, and inflammatory cytokine functions, they cannot completely reduce mortality from severe infections and sepsis. In this study, we focused on the endothelial cell-specific protein, Roundabout 4 (Robo4), which suppresses vascular permeability by stabilizing endothelial cells, and investigated whether enhanced Robo4 expression could be a novel therapeutic strategy against severe infectious diseases. Endothelial-specific overexpression of Robo4 suppresses vascular permeability and reduces mortality in lipopolysaccharide (LPS)-treated mice. Screening of small molecules that regulate Robo4 expression and subsequent analysis revealed that two competitive small molecules against decapentaplegic (SMAD) signaling pathways, activin receptor-like kinase 5 (ALK5)-SMAD2/3 and ALK1-SMAD1/5, positively and negatively regulate Robo4 expression, respectively. An ALK1 inhibitor was found to increase Robo4 expression in mouse lungs, suppress vascular permeability, prevent extravasation of melanoma cells, and decrease mortality in LPS-treated mice. The inhibitor suppressed severe acute respiratory syndrome coronavirus 2 (SARS-CoV-2)-induced endothelial barrier disruption and decreased mortality in mice infected with SARS-CoV-2. These results indicate that enhancing Robo4 expression is an efficient strategy to suppress vascular permeability and mortality in severe infectious diseases, including COVID-19, and that small molecules that upregulate Robo4 can be potential therapeutic agents against these diseases.

Roundabout 4 | vascular permeability | infectious disease | COVID-19 | SMAD

Infectious diseases are induced by the following processes: exposure to pathogens, activation of immune cells, production of inflammatory cytokines, and induction of vascular hyperpermeability. The first three processes can be regulated by established effective drugs, including antipathogenic drugs, steroids, and antibodies against cytokines and their receptors. However, no drugs directly suppress vascular hyperpermeability. Vascular hyperpermeability promotes the recruitment of immune cells and elimination of pathogens under physiological conditions. However, excessive vascular hyperpermeability in severe infectious diseases and sepsis induces severe vascular leakage and edema in multiple organs, resulting in fatal conditions, such as acute respiratory distress syndrome (ARDS).

Vascular permeability is regulated by endothelial cells (ECs), which cover the inner surface of the vasculature. Endothelial permeability is regulated by cell-cell junctions, including adherens and tight junctions. Adherens junctions are regulated by cadherins and nectins, whereas tight junctions are composed of occludin, claudins, and junctional adhesion molecules (1–3). Among these transmembrane proteins, vascular endothelial cadherin (VE-cadherin), which is specifically expressed in ECs, plays a crucial role in endothelial barrier regulation. VE-cadherin-mediated junctions are dissociated by VE growth factor (VEGF) and other inflammatory cytokines, including tumor necrosis factor- α (TNF- α) (4–6). VEGF and TNF- α lead to severe and sometimes fatal organ dysfunction in severe infectious diseases. Neutralization of these factors decreases vascular permeability and mortality in mouse models of endotoxemia and sepsis (1, 7–9). Therefore, molecules that stabilize VE-cadherin-mediated junctions may be novel drugs to suppress the pathology of severe infectious diseases.

One of the promising targets for stabilizing VE-cadherin-mediated junctions is Roundabout 4 (Robo4). Robo4 is specifically expressed in ECs and stabilizes the vasculature

Significance

Due to increased exposure to various infectious diseases, including COVID-19, there is an urgent need for novel drugs that reduce mortality from severe infectious diseases. Although current drugs can suppress pathogen reproduction, immune cell activation, and inflammatory cytokine functions, these cannot effectively reduce mortality from severe infectious diseases. In this study, we focused on the endothelial cell-specific protein Roundabout4 (Robo4) that ameliorates vascular permeability in inflammation. We demonstrated that Robo4 upregulation suppresses vascular permeability and mortality in severe infectious diseases. Moreover, we also demonstrated that small molecules which enhance Robo4 expression suppress vascular permeability and mortality. Our study thus characterizes a novel therapeutic strategy against severe infectious disease that targets vascular permeability.

This article is a PNAS Direct Submission.

Copyright © 2023 the Author(s). Published by PNAS. This open access article is distributed under [Creative Commons Attribution-NonCommercial-NoDerivatives License 4.0 \(CC BY-NC-ND\)](https://creativecommons.org/licenses/by-nc-nd/4.0/).

¹To whom correspondence may be addressed. Email: okadabos@phs.osaka-u.ac.jp.

This article contains supporting information online at <https://www.pnas.org/lookup/suppl/doi:10.1073/pnas.2213317120/-/DCSupplemental>.

Published January 12, 2023.

(10, 11). Robo4 improves the survival rate in mouse infection and endotoxemia models by suppressing vascular hyperpermeability (12, 13). Robo4 also inhibits tumor metastasis by suppressing vascular permeability (14, 15). Robo4 suppresses endothelial hyperpermeability induced by VEGF and TNF- α through multiple mechanisms via interacting proteins, including Slit2, Unc5B, and TRAF7 (12, 16, 17). Interestingly, a previous report showed that down- or up-regulation of Robo4 expression in ECs enhanced or suppressed TNF α -induced endothelial hyperpermeability, respectively, suggesting that vascular permeability can be regulated by controlling Robo4 expression levels (12). Furthermore, the histone deacetylase (HDAC) inhibitor, MS-275 that decreases endothelial Robo4 expression, enhances vascular permeability and tumor metastasis in mouse lungs, indicating that small molecules which regulate Robo4 expression can control vascular permeability and disease (14). Based on this information, we hypothesized that Robo4 overexpression could be a novel therapeutic strategy to ameliorate severe infectious diseases and sepsis by suppressing vascular permeability, and small molecules that enhance Robo4 expression can be potential drugs against these diseases.

In this study, we investigated the effects of Robo4 overexpression on vascular hyperpermeability and mortality induced by lipopolysaccharide (LPS) injection using EC-specific conditional Robo4 overexpression mice. We also investigated a signaling pathway that regulates Robo4 expression by screening a drug library and identified two competitive SMAD signaling pathways as regulators of Robo4 expression. Finally, we demonstrated that an inhibitor of ALK1-SMAD signaling upregulated Robo4 expression, suppressed vascular permeability, prevented extravasation of melanoma cells, and reduced mortality in LPS-injected mice. In addition, the inhibitor suppressed severe acute respiratory syndrome coronavirus 2 (SARS-CoV-2)-induced endothelial barrier disruption and reduced the mortality of SARS-CoV-2-infected mice. Thus, we successfully demonstrated that Robo4-mediated suppression of vascular permeability is an effective strategy to improve the mortality of severe infectious diseases and that small molecules which enhance Robo4 expression are useful drugs for these diseases.

Results

Endothelial-Specific Robo4 Overexpression Suppresses Mouse Endotoxemia and Experimental Metastasis Models. We have previously demonstrated that Robo4 knockout in mice increases LPS-induced vascular permeability and mortality and increases lung colony number in experimental metastasis models (12, 14). To investigate the effects of Robo4 overexpression in these mouse models, we generated inducible endothelial-specific Robo4 overexpression mice (Robo4^{iEC} mice) (Fig. 1A). The injection of Robo4^{iEC} mice with tamoxifen induced Robo4 overexpression in multiple organs (Fig. 1B), indicating the establishment of an EC-specific conditional Robo4 expression in mice. Then, we investigated the effect of induced Robo4 expression on vascular permeability in the lungs using LPS injection and experimental metastasis models. LPS injection in Robo4^{iEC} mice showed decreased vascular leakage of Evans blue in the lungs (Fig. 1C). Intravenous injection of B16-F10 melanoma cells into Robo4^{iEC} mice showed reduced extravasation of the cells from blood vessels to the lungs (Fig. 1D). These results indicate that Robo4 overexpression suppresses vascular permeability in the lungs. In addition, Robo4^{iEC} mice injected with LPS showed an improved survival rate (Fig. 1E). These results indicate that Robo4 overexpression suppresses vascular permeability and mortality during systemic inflammation, which is also induced in severe infectious diseases.

Identification of a Potential Signaling Regulating Robo4 Expression by Drug Screening. To investigate the signaling pathways that regulate Robo4 expression, we established a drug screening system using a mouse EC line, MS1 cells. MS1 cells were stably transfected with luciferase transgene cassettes, including human Robo4 and SV-40 promoter-luciferase, to generate MS1-Robo4 and MS1-SV40 cells (Fig. 2A). Using these cell lines, we established a screening system to identify small molecules that regulate the activity of the Robo4 promoter but not the control SV-40 promoter. Inhibitors of HDAC (Trichostatin A (TSA)) and NF- κ B (ammonium pyrrolidine dithiocarbamate (APDC)), which are known Robo4 suppressors (14), suppressed the luciferase activity of MS1-Robo4 but not that of MS1-SV40 (Fig. 2B), indicating that the screening system functions efficiently. Using this system, we screened 1,280 small molecules from the LoPac library (Fig. 2C) and identified seven candidates that potentially decreased Robo4 promoter activity. Among these, three molecules, IPA-3 (PAK-1 inhibitor), GR127935 (5-HT1b/1D antagonist), and SB-525334 (ALK5 inhibitor) decreased Robo4 expression in human umbilical vein ECs (HUVECs) (Fig. 2D). These results indicate that the signaling pathways associated with PAK-1, 5-HT1b/1D, and ALK5 are potential regulators of Robo4 expression. We focused on ALK5, which regulates transforming growth factor- β (TGF- β)-SMAD signaling because it has been shown to be associated with endothelial permeability (18).

TGF- β Activates Robo4 Expression in a Culture Condition-Dependent Manner. ALK5 is known to be a TGF- β receptor that activates its downstream SMAD2/3. To investigate the regulatory mechanism of Robo4 expression by SMAD2/3, HUVECs were transfected with Small Interfering RNA (siRNAs) for SMAD2/3. Knockdown of SMAD2/3 decreased Robo4 expression in HUVECs (Fig. 3A). This result suggests that the canonical TGF- β -ALK5-SMAD2/3 pathway regulates Robo4 expression, and that the pathway is already activated in this culture condition without TGF- β stimulation (known as the normal condition). Consistent with this, TGF- β 1/2 treatment did not alter Robo4 expression in HUVECs (Fig. 3B). Therefore, we searched for culture conditions in which TGF- β -ALK5-SMAD2/3 signaling was suppressed and found a Matrigel culture condition (*SI Appendix, Fig. S1A*). Under this condition, the expression of plasminogen activator inhibitor-1 (PAI-1) which is enhanced by TGF- β -ALK5-SMAD2/3 signaling (19, 20) was suppressed, (*SI Appendix, Fig. S1B*). Robo4 expression was also suppressed compared to that under normal conditions (*SI Appendix, Fig. S1B*), and TGF- β 1/2 treatment increased Robo4 expression (Fig. 3B). Taken together, these results indicate that TGF- β -ALK5-SMAD2/3 signaling promotes Robo4 expression (Fig. 3G).

BMP9-ALK1-SMAD1/5 Signaling Suppresses Robo4 Expression. In addition to the suppression of ALK5 signaling, we also found that Matrigel increased the expression of inhibitor of differentiation-1 (ID-1), which is enhanced by ALK1 signaling, a competitive signaling pathway of ALK5 signaling (19, 20) (*SI Appendix, Fig. S1B*). We hypothesized that ALK1 signaling also regulates Robo4 expression. Since ALK1-SMAD1/5 signaling has been shown to be activated by bone morphogenetic protein 9 (BMP9) in ECs (21), we investigated whether BMP9-ALK1-SMAD1/5 signaling regulates Robo4 expression. BMP9 treatment suppressed Robo4 expression in HUVECs cultured under normal conditions (Fig. 3C). BMP9-induced Robo4 suppression was inhibited by siRNA-mediated knockdown of SMAD1/5 (Fig. 3D). Similarly, the ALK1 inhibitor K02288 inhibited BMP9-mediated Robo4 suppression (Fig. 3E and *SI Appendix, Fig. S2*). K02288 increased

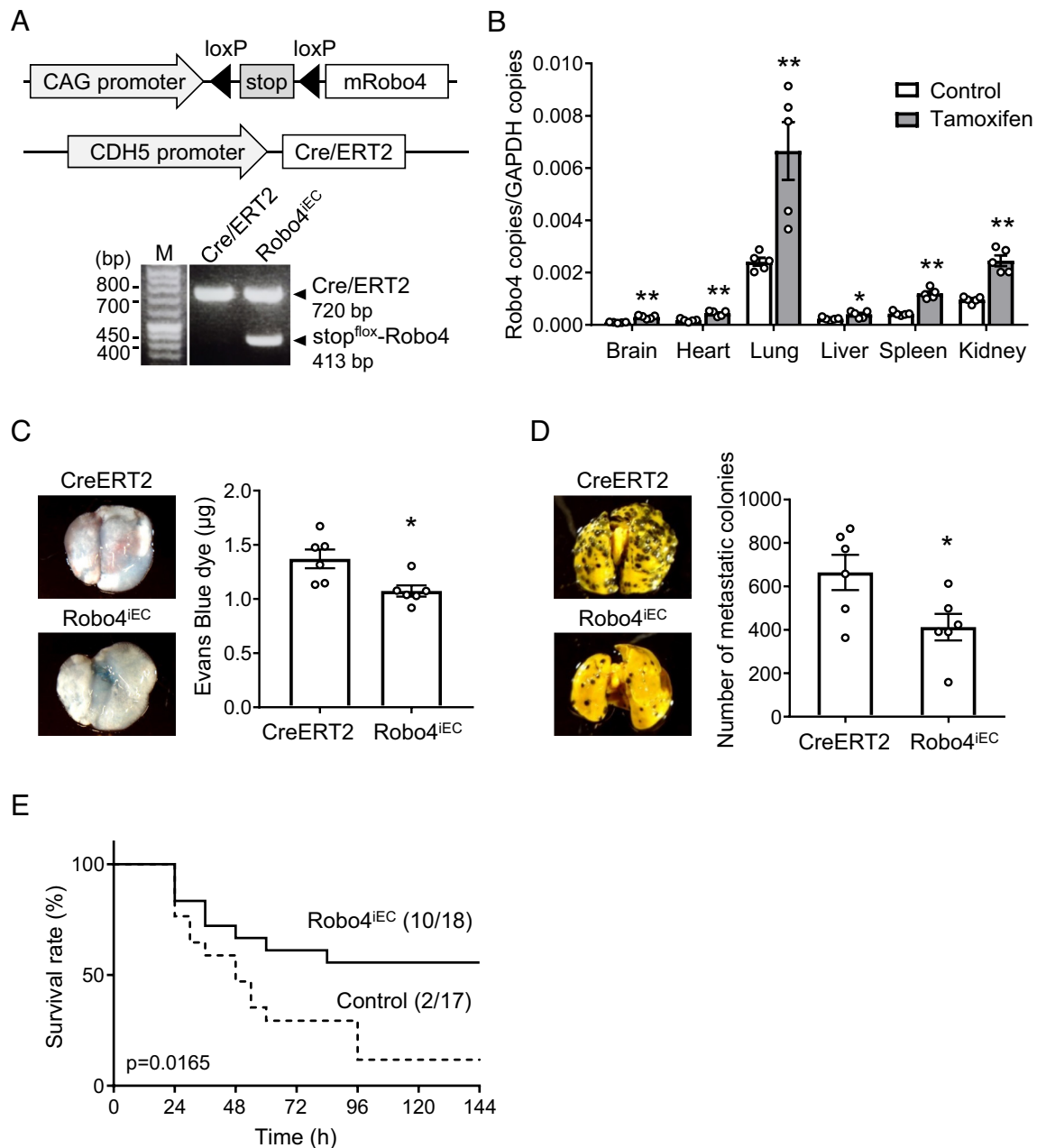


Fig. 1. Endothelial-specific Robo4 overexpression suppresses LPS-induced mortality and melanoma cell migration in mice. (A) Transgenes and genotyping results of Robo4^{IEC} mice. CDH5 promoter induces endothelial-specific expression of Cre/ERT2. Tamoxifen activates Cre/ERT2 and induces deletion of the floxed Stop codon and CAG promoter-driven mRobo4 overexpression. (B) Expression level of Robo4 mRNA in the organs of Robo4^{IEC} mice treated with tamoxifen (n = 5, *P < 0.05, **P < 0.01 by the unpaired t test) (C) Vascular permeability in the lungs in the Robo4^{IEC} and control (CDH5-Cre/ERT2) mice. (n = 6, *P < 0.05 by the unpaired t test) (D) Experimental metastasis models using Robo4^{IEC} and control mice treated with tamoxifen. B16-F10 melanoma cells were intravenously injected, and metastasized colonies were counted (n = 6, *P < 0.05 by the unpaired t test). (E) Survival study using LPS-injection models in Robo4^{IEC} and control mice treated with tamoxifen (control: n = 18, Robo4^{IEC}: n = 17; P = 0.017 by the log-rank test) Data are expressed as the mean ± SEM.

Robo4 expression in HUVECs cultured under Matrigel but not under the normal condition (Fig. 3F). These results indicate that BMP9-ALK1-SMAD1/5 signaling suppresses Robo4 expression (Fig. 3G) and that K02288 is a potential small molecule that increases Robo4 expression in vivo.

ALK1 Inhibitor Increases Robo4 and Suppresses Vascular Hyperpermeability in the Mouse Lung. To investigate whether K02288 increased Robo4 expression in mice, we analyzed the basal expression levels and expression pattern of ALK1 in mouse organs. ALK1 expression is particularly high in the lungs when compared to that in other organs (Fig. 4A), suggesting that

K02288 predominantly affects the lungs. Immunofluorescent staining for ALK1 and VE-cadherin showed that ALK1 is mainly expressed in ECs in the mouse lung vasculature (SI Appendix, Figs. S3 and S4). We intravenously injected mice with K02288 and analyzed Robo4 expression in the lungs and kidneys. K02288 significantly increased Robo4 expression in the lungs but not in the kidneys (Fig. 4B), where ALK1 expression was low (Fig. 4A). Consistent with this, K02288 suppressed vascular leakage of Evans blue in the lungs of LPS-injected wild-type mice, but not in the kidneys (Fig. 4C). In contrast, K02288 did not affect vascular leakage in the lungs and kidneys in Robo4^{-/-} mice (Fig. 4D). In addition, K02288 decreased the

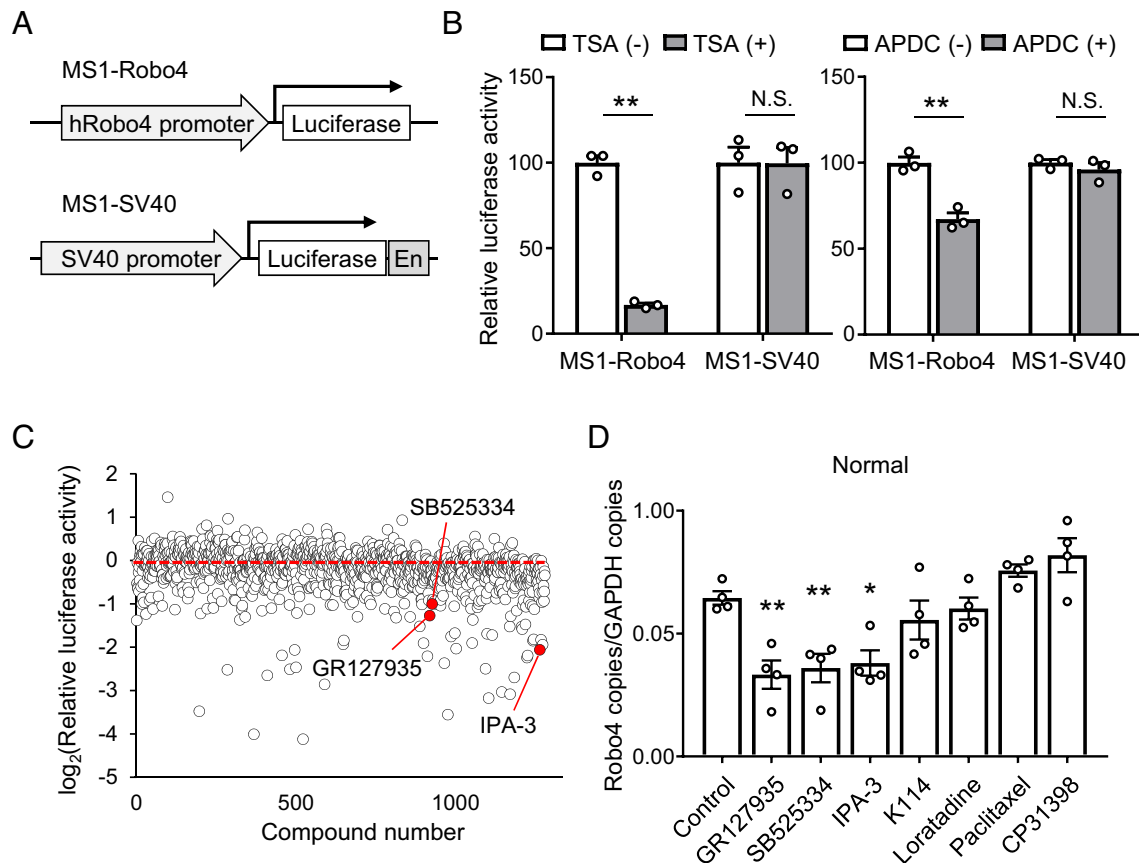


Fig. 2. Screening for small molecules regulating Robo4 expression in ECs. (A) Two MS1 cell lines used for screening. Mouse EC line (MS1) cells were stably transfected with luciferase gene driven by human Robo4 promoter or SV-40 promoter with enhancer (En). (B) Effect of known Robo4 suppressor on luciferase activity in cell lines. Inhibitors for histone deacetylase (TSA) and NF- κ B (APDC) specifically suppressed luciferase activity in MS1-Robo4 ($n = 4$, $^{**}P < 0.01$ by the unpaired t test). (C) Screening results for LoPac library using cell lines. Data expressed as relative promoter activity (Robo4 promoter activity/SV40 promoter activity). (D) Robo4 expression levels in HUVECs treated with candidates from the screening ($n = 4$, $^{*}P < 0.05$, $^{**}P < 0.01$ by Dunnett's test). Data are expressed as the mean \pm SEM.

extravasation of melanoma cells in the lungs of wild-type mice but not in Robo4^{-/-} mice (Fig. 5 A and B), indicating the Robo4-dependent effect of K02288. Taken together, these results indicate that K02288 increases Robo4 expression and suppresses vascular permeability in mouse lungs.

ALK1 Inhibitor Ameliorates Mortality of the Mouse LPS and COVID-19 Models. We investigated the effect of K02288 on the survival of LPS-injected mice. K02288 pretreatment significantly decreased the mortality rate in LPS-injected mice but not in Robo4^{-/-} mice (Fig. 5 C and D). These results indicated that K02288 pretreatment ameliorated the pathological phenotype and improved the survival of LPS-injected mice in a Robo4-dependent manner.

Finally, we investigated the effect of K02288 on SARS-CoV-2-induced endothelial barrier disruption by using an airway-on-a-chip (Fig. 6A). This chip includes airway epithelial cells and lung microvascular ECs in the top (airway channel) and bottom (vascular channel) channels, respectively, and mimics the lung microenvironment. We have demonstrated that SARS-CoV-2 replicates in epithelial cells of the airway channel and migrates to the vascular channel by disrupting the endothelial barrier (22). K02288 treatment reduced SARS-CoV-2 migration to the vascular channel without affecting the copy number of SARS-CoV-2 in the airway channel (Fig. 6B). Consistently, K02288 treatment suppressed the SARS-CoV-2-induced disruption of VE-cadherin junctions (Fig. 6C). These results indicate that K02288 treatment suppresses SARS-CoV-2-mediated endothelial barrier disruption.

Then, we investigated the effects of K02288 on SARS-CoV-2-infected mice. SARS-CoV-2 infection hardly changed the EC-specific expression pattern of ALK1 in the lungs (*SI Appendix, Figs. S3*). Intraperitoneal injection of K02288 increased Robo4 expression in SARS-CoV-2-infected mice (Fig. 6D) and improved the survival rate by suppressing the decrease in body weight (Fig. 6E and *SI Appendix, Fig. S4 A and B*). K02288 did not alter the expression of junction-related proteins and junction structures (*SI Appendix, Fig. S4 C and D*). Taken together, K02288 suppressed endothelial hyperpermeability and mortality in both airway-on-a-chip and mouse coronavirus disease 2019 (COVID-19) models.

Discussion

Existing drugs targeting pathogens, immune cells, and inflammatory cytokines effectively suppress the pathological phenotype of severe infectious diseases but cannot sufficiently suppress their mortality rate. In this study, we demonstrated that Robo4 overexpression suppresses vascular permeability and mortality in LPS-injected mice. Through the analysis of the signaling pathway that regulates Robo4 expression, we found that two competing SMAD signaling pathways positively and negatively regulate Robo4 expression. In addition, we demonstrated that the ALK1 inhibitor K02288 functions as an enhancer of Robo4 expression, suppresses vascular permeability, prevents extravasation of melanoma cells, and suppresses mortality in LPS-injected and SARS-CoV-2-infected mice. Thus, we

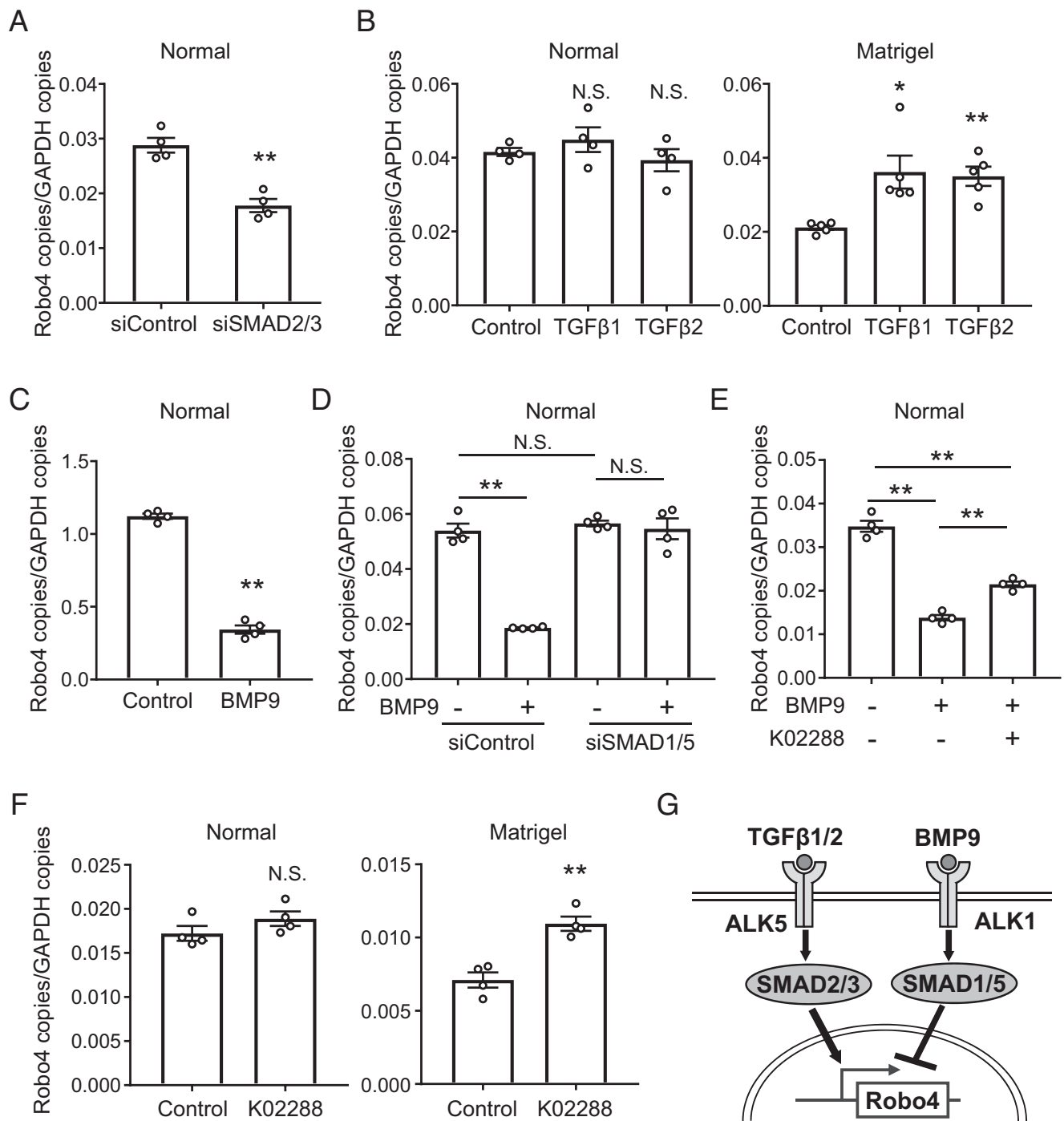


Fig. 3. Competitive SMAD signaling pathways regulate Robo4 expression both positively and negatively. (A) Robo4 expression levels in HUVECs treated with siRNA for SMAD2 and SMAD3 ($n = 4$, $**P < 0.01$ by the unpaired t test). (B) Robo4 expression level in TGF- β 1/2-treated HUVECs under normal ($n = 4$) or Matrigel conditions ($n = 5$, $*P < 0.05$, $**P < 0.01$ by Dunnett's test). (C) Robo4 expression levels in HUVECs treated with BMP9 ($n = 4$, $**P < 0.01$ by the unpaired t test). (D) Robo4 expression levels in HUVECs treated with BMP9 and siRNA for SMAD1 and SMAD5 ($n = 4$, $**P < 0.01$; N.S., not significant by Tukey's test). (E) Robo4 expression levels in HUVECs treated with K02288 and BMP9 ($n = 4$, $**P < 0.01$ by Tukey's test). (F) Robo4 expression levels in HUVECs cultured in Matrigel containing K02288 ($n = 4$, $**P < 0.01$; N.S., not significant by the unpaired t test). (G) Schematic illustration of positive and negative Robo4 regulation by TGF- β -ALK5-SMAD2/3 and BMP9-ALK1-SMAD1/5 signaling pathways. Data are expressed as the mean \pm SEM.

successfully demonstrated that Robo4-mediated suppression of vascular hyperpermeability is an effective therapeutic strategy against severe infectious diseases and identified the ALK1 inhibitor as a drug that inhibits vascular permeability by increasing Robo4 expression.

London et al. previously demonstrated that Robo4 signaling ameliorates mortality and cytokine storms in sepsis and influenza (13). Importantly, this study proposed that the suppression of vascular permeability could be a novel strategy against the

mortality of severe infectious diseases induced by various types of pathogens, including bacteria and viruses, and could be applied to infectious diseases induced by novel pathogens that arise in the future. In the study by London et al., they used a Robo4 ligand, Slit2, to activate the downstream signaling of Robo4 (17). However, it is still unclear whether Slit2 is a ligand for Robo4 because Robo4 lacks a Slit2 binding domain that is involved in other Robo family proteins, and direct interaction between Robo4

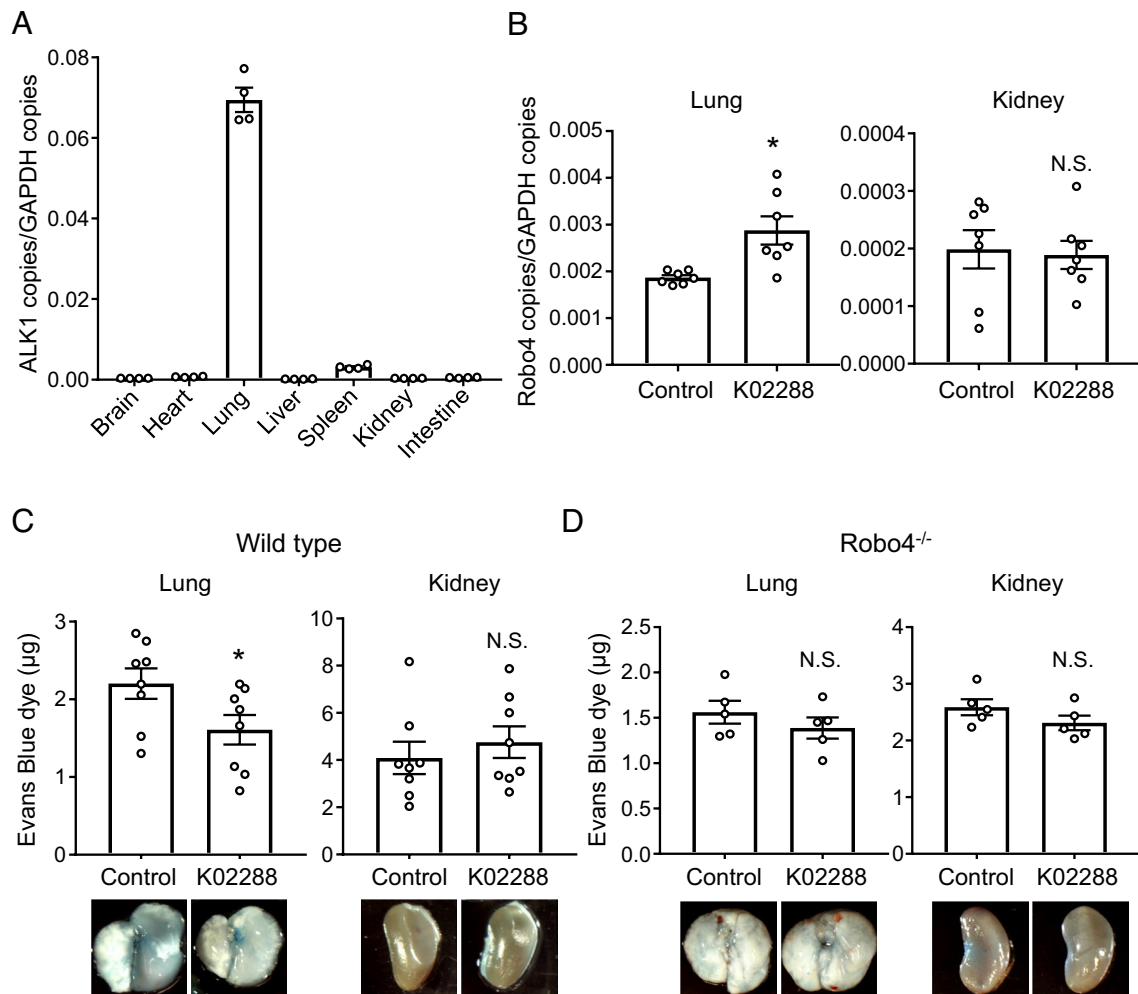


Fig. 4. ALK1 inhibitor increased Robo4 expression and suppresses LPS-induced vascular permeability in mice. (A) ALK1 expression levels in organs of C57BL/6 mice ($n = 4$). (B) Robo4 expression levels in lungs and kidneys of wild-type (C57BL/6N) mice treated with or without K02288 ($n = 7$, $*P < 0.05$, N.S., not significant by the unpaired t test). (C) Vascular permeability assay using wild-type mice treated with or without K02288. Extravasated Evans blue in lungs and kidneys was quantified. ($n = 8$, $*P < 0.05$; N.S., not significant by the unpaired t test). (D) Vascular permeability assay using Robo4^{-/-} mice treated with or without K02288. Extravasated Evans blue in lungs and kidneys was quantified. ($n = 5$, N.S., not significant by the unpaired t test). Pictures are representative images of the lungs and kidneys. Data are expressed as the mean \pm SEM.

and Slit2 has not been detected in some assays (16, 23, 24). In addition, Robo4 was shown to stabilize the vasculature through two other mechanisms. The second mechanism is that Robo4 in the plasma membrane functions as a ligand for the netrin receptor Unc5B and transmits a stabilizing signal to the adjacent ECs (16, 24). Finally, Robo4 interacts with TRAF7 and suppresses vascular permeability during inflammation. In the current study, we adopted a strategy to increase Robo4 expression in ECs because it then enhances Robo4 function via all three mechanisms.

We demonstrated that Robo4 expression is positively and negatively regulated by TGF- β -ALK5-SMAD2/3 and BMP9-ALK1-SMAD1/5 signaling, respectively. Previous reports have indicated that TGF- β -ALK5 signaling maintains a quiescent endothelium. For example, TGF- β -ALK5-SMAD2/3 signaling inhibits angiogenesis by suppressing EC proliferation, tube formation, and migration (20, 25). This signaling pathway also induces PAI-1 as a negative regulator of EC migration (26). In this context, the upregulation of Robo4 by TGF- β -ALK5-SMAD2/3 signaling seems reasonable because Robo4 stabilizes ECs by suppressing endothelial migration (11, 17). In contrast, ALK1 signaling regulates EC function in context- and ligand-dependent manners. TGF- β -stimulated ALK1 signaling induces EC migration and proliferation via SMAD1/5 activation (25). However, other

reports have demonstrated that ALK1 signaling stimulated by TGF- β or BMP9 inhibits EC migration and angiogenesis (21, 27–29). Similarly, BMP9 has been shown to positively and negatively regulate vascular permeability (30, 31). In our study, K02288 suppressed vascular permeability, indicating that ALK1 contributed to the enhancement of vascular permeability. However, it is not clear what the major ligand of ALK1 is and how ALK1 promotes vascular hyperpermeability in endotoxemia models. Further studies are needed to understand the pathological significance of ALK1 signaling in severe infectious diseases. In addition, it is necessary to investigate the physiological significance of the culture-condition-dependent switching mechanism of SMAD signaling and how this mechanism regulates Robo4 expression.

Moreover, even the high concentration of K02288 could not completely compensate for the BMP9-induced Robo4 suppression in HUVECs (Fig. 3E and *SI Appendix, Fig. S2*). In contrast, the high concentration of K02288 suppressed BMP9-induced ID-1 expression by inhibiting ALK1 signaling (*SI Appendix, Fig. S2*). These results suggest that K02288 has a different effect that decreases Robo4 by other mechanisms in addition to the main effect that increases Robo4 by inhibiting ALK1 signaling. Further investigation of the mechanism that induces the other effect of

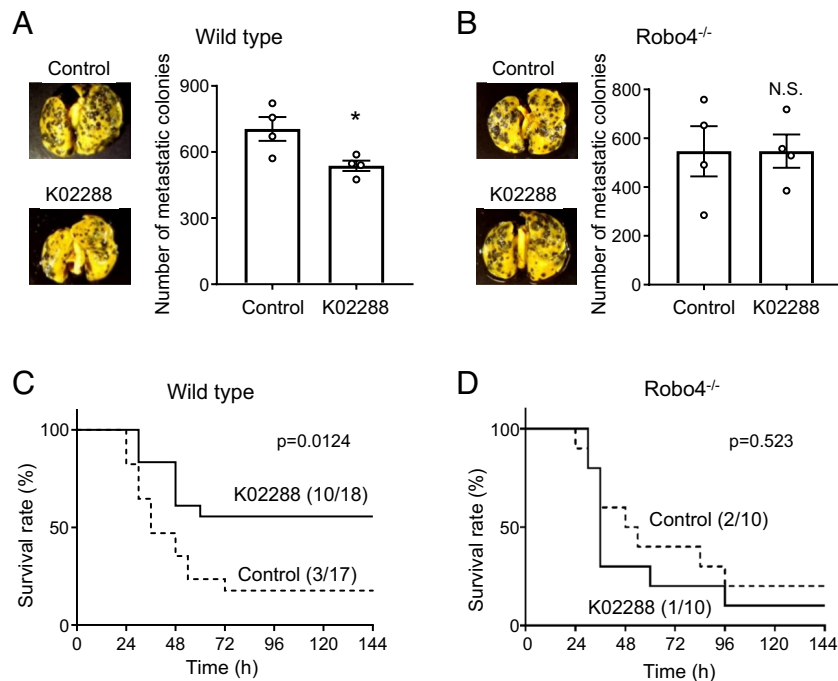


Fig. 5. ALK1 inhibitor ameliorates LPS-induced mortality and experimental metastasis of melanoma cells in mice. (A) Lung colony number in the experimental metastasis models using wild-type mice treated with or without K02288. (n = 4, * $P < 0.05$ by the unpaired t test). (B) Lung colony number in the experimental metastasis models using $Robo4^{-/-}$ mice treated with or without K02288. (n = 4, N.S., not significant by the unpaired t test). (C) Survival study of LPS-injected wild-type (C57BL/6N) mice treated with or without K02288 (control: n = 17, K02288: n = 18; $P = 0.012$ by the log-rank test). (D) Survival study using LPS-injected $Robo4^{-/-}$ mice treated with or without K02288 (n = 10; $P = 0.523$ by the log-rank test). Data are expressed as the mean \pm SEM.

K02288 and generation of ALK1 inhibitors without the side effect may be important for developing drugs that efficiently increase Robo4 expression and suppress inflammatory diseases.

Our results and those of previous reports indicate that ALK1 is specifically and highly expressed in lung ECs (32). Consistently, K02288 promoted Robo4 expression and suppressed vascular permeability in the lungs, but not in the kidneys. These results suggest that K02288 mainly affects pulmonary ECs and suppresses endothelial permeability in the lungs and mortality due to endotoxemia. In this regard, ALK1 could be a useful therapeutic target for lung injury in severe infectious diseases, as it induces fewer side effects in other organs.

K02288 suppresses SARS-CoV-2-mediated human endothelial barrier disruption in the airway-on-a-chip. In contrast, severe destruction of endothelial junction structure was hardly observed in SARS-CoV-2-infected mice. These infection model-dependent results were partially derived due to the difference of species, since it has been reported that mouse SARS-CoV-2 infection models have their own limitations and cannot completely mimic the severe phenotype of COVID-19 (33). Further improvement of the mouse SARS-CoV-2 infection model is required to clearly show the effects of K02288 on vascular permeability.

Our screening system identified small molecules that suppress Robo4 expression: IPA-3 (PAK-1 inhibitor), GR127935 (5-HT1b/1D antagonist), and SB-525334 (ALK5 inhibitor). These results suggest that PAK-1 and 5-HT1b/1D are also involved in the regulation of Robo4 expression, in addition to SMAD signaling, which we focused on in this study. Regulation of Robo4 expression by signaling mediated by PAK-1 and 5-HT1b/1D has not yet been reported. These signaling pathways, along with SMAD signaling, may contribute to the generation of other small molecules that increase Robo4 expression.

In conclusion, we demonstrated that suppressing vascular permeability by targeting Robo4 could be a novel therapeutic strategy

against sepsis and severe infectious diseases and that small molecules that increase Robo4 expression can be potential and effective drugs to suppress these diseases. New drugs targeting vascular permeability in combination with existing drugs could contribute to the reduction of mortality in patients with severe infectious diseases induced by preexisting and emerging infectious diseases.

Materials and Methods

Generation and Culture of Cell Lines. HUVECs (Lonza) were cultured in an microvascular endothelial cell growth medium-2 (EGM-2MV; Lonza). For the generation of screening cell lines MS1-Robo4 and MS1-SV40, the puromycin-resistant gene was amplified from the pTRE2pur vector (Takara Bio) by PCR using primers (SI Appendix, Table S1) and inserted into the plasmids pGL3-Robo4 (34) and pGL3-Control (Promega) using the In-Fusion HD Cloning Kit (Takara Bio). The resulting plasmids were linearized by digestion with *Asel* and stably transfected into MS1 cells using Lipofectamine 2000 (Invitrogen). Forty-eight hours after transfection, stably transfected cells were selected by culturing with puromycin (0.8 μ g/mL) for 18 d. Established cells (MS1-Robo4 and MS1-SV40) and the mouse melanoma cell line B16-F10 (American Type Culture Collection) were cultured in Dulbecco's modified eagle medium (DMEM; Nacalai Tesque) containing 10% fetal bovine serum (FBS), 100 U/mL penicillin, and 100 μ g/mL streptomycin. All the cells were cultured in a humidified atmosphere with 5% CO_2 at 37 $^{\circ}C$.

Screening of the Drug Library. For the validation of the screening cell lines, MS1-Robo4 or MS1-SV40 cells were treated with TSA (150 nM; FUJIFILM) or APDC (80 nM; SIGMA) for 24 h. For the screening, MS1-Robo4 or MS1-SV40 (5×10^3 cells) were seeded on 384 well black plates (Corning) using Multi Drop (Tecan) and cultured for 24 h. The cells were treated with small molecules (10 μ M) from the Library of Pharmacologically Active Compounds 1280 (LoPac1280, Sigma) for 24 h. Luciferase activity was measured using an FDSS7000 (Hamamatsu Photonics) and the Steady-Glo Luciferase Assay System (Promega).

Treatment of HUVECs with Small Molecules and Cytokines. HUVECs were treated with small molecules from the LoPac library (10 μ M; GR127935,

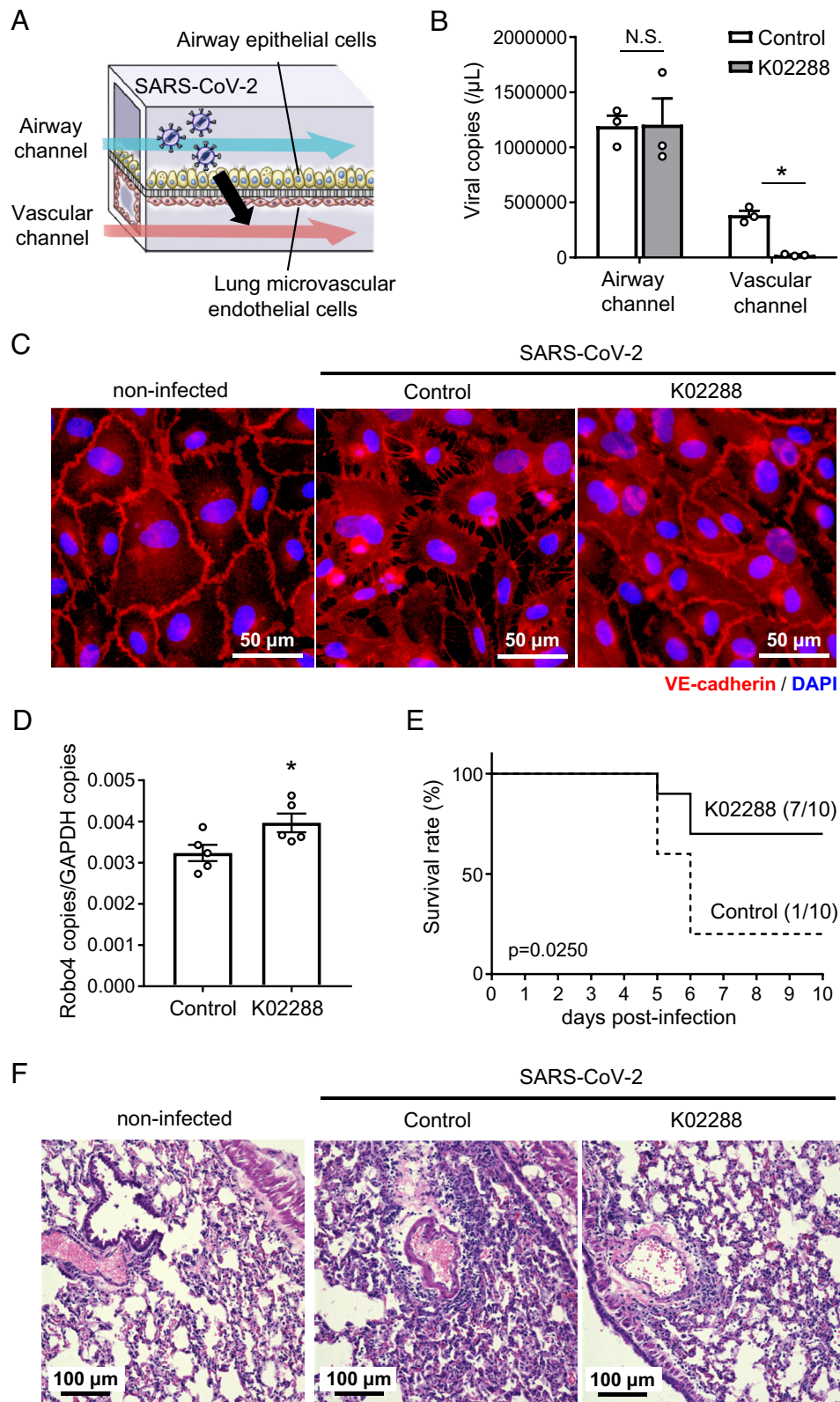


Fig. 6. ALK1 inhibitor suppresses SARS-CoV-2-induced endothelial hyperpermeability and mortality in mice. (A) Schematic illustration of the airway-on-a-chip. Medium containing 0.1 MOI SARS-CoV-2 was injected into the airway channel. The SARS-CoV-2-infected airway-on-a-chips were cultured with the AO differentiation medium (airway channel) and DMSO- or K02288 (1 μM)-containing EGM2-MV medium (vascular channel) for 6 d. (B) Viral copy numbers in the cell culture supernatant of the airway and vascular channels ($*P < 0.05$ by the unpaired *t* test). (C) Immunofluorescent staining for VE-cadherin in the lung microvascular ECs in the airway-on-a-chip. (D) Robo4 expression levels in lungs of SARS-CoV-2 infected BALB/c mice treated with or without K02288 ($n = 5$, $*P < 0.05$ by the unpaired *t* test). (E) Survival study of SARS-CoV-2-infected BALB/c mice treated with or without K02288 (control: $n = 10$, K02288: $n = 10$; $P = 0.025$ by the log-rank test). We defined the day that mice had less than 75% of the initial body weight as the day of death. (F) Representative images of hematoxylin and eosin-stained lung sections from SARS-CoV-2-infected mice with or without K02288 treatment and noninfected mice. Data are expressed as the mean \pm SEM.

SB525334, IPA-3, K114, loratadine, paclitaxel, and CP31398) or K02288 (1 μ M; Cayman Chemical) and incubated for 24 h. For the cytokine treatment, HUVECs were cultured in a serum-starved medium (endothelial cell basal medium-2 (EBM-2; Lonza) containing 0.5% FBS) for 16 h and treated with TGF- β 1 or TGF- β 2 (5 ng/mL; R&D systems) for 24 h or BMP9 (1 ng/mL; R&D systems) for 6 h. For the treatment with a small molecule and a cytokine, HUVECs were treated with K02288 (0.1 to 2 μ M) for 30 min and then with BMP9 (1 ng/mL).

Culture of HUVECs in Matrigel. Matrigel (Corning), diluted in EBM-2, was plated and incubated for 30 min at 37 °C. HUVECs were seeded on Matrigel, incubated for 24 h, and treated with TGF- β 1, TGF- β 2 (5 ng/mL), or K02288 (1 μ M) for 24 h. The cells were harvested using Cell Recovery Solution (Corning).

siRNA-Mediated SMAD Knockdown. siRNAs against SMAD1 (VHS41097), SMAD2 (VHS41107), SMAD3 (s8401), SMAD5 (VHS41124), and control siRNAs (Stealth RNA siRNA Negative Control Med GC Duplex #2) were purchased from Thermo Fisher Scientific and used for the knockdown experiments (10 nM for SMAD1/5, 20 nM for SMAD2, and 5 nM for SMAD3). For the knockdown of SMAD2/3 or SMAD1/5, HUVECs were transfected with siRNAs using Lipofectamine RNAi-Max (Invitrogen) and incubated for 24 or 48 h, respectively. The cells transfected with SMAD1/5 siRNA were cultured in a serum-starved medium for 16 h and treated with BMP9 (1 ng/mL) for 6 h.

Generation of Robo4 Overexpression and Deficient Mice. A mouse Robo4 cDNA fragment was amplified using PCR and inserted into the pCAG-stop^{fllox} vector (#51269; Addgene) (35). The transgene fragment (cytomegalovirus-immediate early enhancer/chicken b-actin/rabbit b-globin (CAG) promoter-stop^{fllox}-mRobo4) was isolated from the plasmid, introduced into a fertilized egg of a C57BL/6 mouse by microinjection, and transplanted into pseudopregnant mice to establish a CAG-stop^{fllox}-Robo4 mouse. CAG-stop^{fllox}-Robo4 mice were then crossed with CDH5-Cre/ERT2 mice (36) to establish Robo4^{IEC} mice. The generation of Robo4-deficient mice (Robo4^{-/-}) has been previously reported (12). All animal experiments in this study, except for the SARS-CoV-2 infection models, were approved by the ethics committee of Osaka University (approval number: Douyaku-30-11-2).

For the analysis using Robo4^{IEC} mice, male and female Robo4^{IEC} mice (6 wk old) were intraperitoneally injected with tamoxifen (1 mg/mouse; Sigma-Aldrich) in corn oil for 4 consecutive days. Two weeks after the first injection, organs were harvested and used for RNA preparation. For the analysis using K02288-treated mice, male C57BL/6 mice (8 wk old) were intravenously injected with K02288 (0.5 mg/kg body weight) in phosphate-buffered saline (PBS) containing 1% dimethyl sulfoxide (DMSO) or vehicle. Twenty-four hours later, the lungs and kidneys were harvested and used for RNA preparation.

qRT-PCR. Total RNA from cells or organs was prepared using the RNeasy Mini Kit (Qiagen), the FastGene RNA Basic Kit (NIPPON Genetics), or ISOGEN (NIPPON GENE). RNA was reverse-transcribed using Superscript VIL0 Master Mix (Invitrogen). Real-time RT-PCR was performed using the QuantiTect SYBR Green PCR Kit (Qiagen) and specific primers (*SI Appendix, Table S1*) using a CFX384 Touch Real-Time PCR Detection System (Bio-Rad). Copy numbers were calculated from a standard curve prepared using known amounts of plasmids, including the target sequences, or the relative quantitation of target mRNA levels was performed using the 2^{- $\Delta\Delta$ CT} method. The expression levels of the genes were normalized to GAPDH levels.

Survival Study Using LPS-Injected Mice. Robo4^{IEC} or CDH5-Cre/ERT2 mice (male, 5 to 6 wk old) were intraperitoneally injected with tamoxifen (1 mg/mouse; Sigma-Aldrich) in corn oil for four consecutive days. Two weeks after the first injection, the mice were intraperitoneally injected with LPS (25 mg/kg body weight; Sigma-Aldrich) in PBS. C57BL/6N and Robo4^{-/-} mice (male, 7 to 8 wk old) were intravenously injected with K02288 (0.5 mg/kg body weight) in PBS containing 1% DMSO. Twenty-four hours later, C57BL/6N and Robo4^{-/-} mice were intraperitoneally injected with LPS (8 and 12 mg/kg body weight, respectively). Survival was assessed for 144 h.

Vascular Permeability Assay. Robo4^{IEC} or CDH5-Cre/ERT2 mice (male, 6 wk old) were intraperitoneally injected with tamoxifen (1 mg/mouse) for 2 consecutive days. Ten days after the injection, the mice were intraperitoneally injected with LPS (80 mg/kg body weight). Six hours later, 100 μ L of 1% Evans blue dye in PBS was intravenously administered to the mice. One hour later, the mice were perfused with PBS containing 2 mM ethylenediaminetetraacetic acid (EDTA) during

anesthesia with isoflurane and organs were harvested. Evans blue dye was eluted by incubating the organs in formamide for 2 d. The eluted dye was quantified by measuring its optical density at 620 nm. For the assay using K02288, C57BL/6N and Robo4^{-/-} mice (male, 8 wk old) were intravenously injected with K02288 (0.5 mg/kg body weight). Twenty-four hours after injection, the mice were intraperitoneally injected with LPS (16.5 mg/kg body weight). Six hours later, the mice were injected with Evans blue dye and assayed in a similar manner.

Experimental Metastasis Model. Robo4^{IEC} or CDH5-Cre/ERT2 mice (female, 6 wk old) were intraperitoneally injected with tamoxifen (1 mg/mouse) for three consecutive days. Two weeks after the first tamoxifen injection, mice were intravenously injected with B16-F10 cells (3 \times 10⁵ cells) in PBS containing 0.02% EDTA. After 2 wk, the lungs were harvested and fixed in Bouin's solution. The metastasized melanoma colonies on the lung surface were counted using an SZX7 stereo microscope (Olympus) equipped with a MAS-500 USB camera (Marutsuelec). For the assay using K02288, C57BL/6N and Robo4^{-/-} mice (female, 6 wk old) were intraperitoneally injected with K02288 (2 mg/kg body weight). Twenty-four hours later, the mice were injected with B16-F10 cells and assayed in a similar manner.

Preparation of SARS-CoV-2. The severe acute respiratory SARS-CoV-2 strain B.1.1.214 (GISAID accession number: EPI_ISL_2897162) was isolated from a nasopharyngeal swab sample from a patient with COVID-19. This study was approved by the research ethics committee of the Kyoto University (R2379-3). The virus was proliferated in Vero/TMPRSS2 cells (JCRB1818, JCRB Cell Bank) (37) and stored at -80 °C. Vero/TMPRSS2 cells were cultured in a minimum essential medium (Sigma-Aldrich) supplemented with 5% FBS and 1% penicillin/streptomycin. In vitro experiments using SARS-CoV-2 were performed in a biosafety level 3 facility at Kyoto University, following strict regulations.

Mouse-adopted SARS-CoV-2 (MA10) was prepared by the circular polymerase extension reaction (CPER) method, as described previously (38). The backbone of MA10 is the SARS-CoV-2 National institute of infectious diseases strain (2019-nCoV_Japan_TY_WK-5212020) and MA10 has seven mutations: nsp4: T295I, nsp7: K2R, nsp8: E23G, S: Q493K/Q498Y, P499T, and orf6: F7S, which have been reported by Leist et al. as adaptive mutations introduced in SARS-CoV-2 during serial passages in BALB/c mice (39). Briefly, the virus was amplified in VeroE6/TMPRSS2 cells (JCRB1819; JCRB Cell Bank) and stored at -80 °C. VeroE6/TMPRSS2 cells were cultured in DMEM (high Glucose) (Nacalai Tesque) supplemented with 10% FBS and 1% penicillin/streptomycin. In vivo experiments using MA10 were performed in a biosafety level 3 facility at Osaka University, following strict regulations.

Preparation of Airway-on-a-Chips and SARS-CoV-2 Infection Models. Human lung microvascular ECs (HMVEC-L) were obtained from Lonza and maintained in an EGM-2MV medium (Lonza). To prepare the airway-on-a-chip, the bottom channel (vascular channel) of a polydimethylsiloxane (PDMS) device was precoated with fibronectin (3 μ g/mL, Sigma). The PDMS devices were generated according to our previous report (40). HMVEC-L were suspended at a density of 5 \times 10⁶ cells/mL in an EGM-2MV medium. Ten microliters of the suspension medium were injected into the fibronectin-coated bottom channel of the PDMS device. The PDMS device was then inverted and incubated for 1 h. After 1 h, the device was turned over and the EGM-2MV medium was added to the vascular channel. After 4 d, human airway organoids (AO) were dissociated and seeded into the top channel (airway channel). AO was generated as described in our previous report (41). AO was dissociated into single cells and then suspended at 5 \times 10⁶ cells/mL in AO differentiation medium. Ten microliters of the suspension medium were injected into the top channel. After 1 h, the AO differentiation medium was added to the airway channel. The cells were cultured in a humidified atmosphere containing 5% CO₂ at 37 °C. AO differentiation medium containing SARS-CoV-2 (0.1 MOI) was injected into the airway channel and cultured for 2 h. Infected airway-on-a-chips were cultured with AO differentiation medium (airway channel) and DMSO- or K02288 (1 μ M)-containing EGM-2MV medium (vascular channel) for 6 d. The viral RNA copy numbers in the cell culture supernatants of the airway and vascular channels were measured.

Measurement of Viral RNA Copy Number. The cell culture supernatant was combined with an equal volume of 2 \times RNA lysis buffer (distilled water containing 0.4 U/ μ L SUPERase-In RNase Inhibitor (Thermo Fisher Scientific), 2% Triton X-100, 50 mM KCl, 100 mM Tris-HCl (pH 7.4), and 40% glycerol) and incubated at room

temperature for 10 min. The mixture was diluted 10 times with distilled water. Viral RNA was quantified using a One-Step TB Green PrimeScript PLUS RT-PCR Kit (Perfect Real Time) (Takara Bio) on a QuantStudio 1 Real-Time PCR System (Thermo Fisher Scientific) and specific primers (SI Appendix, Table S1). Standard curves were prepared using SARS-CoV-2 RNA (1×10^5 copies/ μ L) purchased from Nihon Gene Research Laboratories.

Immunofluorescent Staining. The polyethylene terephthalate membrane adhered to the HMVEC-L was mechanically removed from the airway-on-a-chip and used for immunofluorescent staining. The resulting cells were fixed with 4% paraformaldehyde, permeabilized with PBS containing 0.2% Triton X-100, and blocked with PBS containing 2% bovine serum albumin and 10% FBS. The resulting cells were incubated with antibodies against VE-cadherin (F8, Santa Cruz Biotechnology), followed by incubation with secondary antibodies conjugated to Alexa Fluor 594 (Thermo Fisher Scientific). The slides were mounted with ProLong™ Gold Antifade Mountant with DAPI (Thermo Fisher Scientific) and analyzed using BZ-X700 (KEYENCE).

The 1% PFA-fixed mouse lung sections were permeabilized with PBS containing 0.2% Triton X-100 and incubated with antibodies against ALK1 (AF770, R&D Systems) and VE-cadherin (ab282277, Abcam), followed by incubation with secondary antibodies conjugated to Alexa Fluor 488 or Alexa Fluor 546 (Thermo Fisher Scientific). The slides were treated and mounted using a Vector TrueVIEW Autofluorescence Quenching Kit with DAPI (Vector Laboratories) and analyzed using BZ-X700 (KEYENCE).

Survival Study Using SARS-CoV-2-Injected Mice. Male BALB/c mice (8 wk old) were intranasally injected with SARS-CoV-2 (MA10; 2×10^5 PFU/mouse). K02288 (2 mg/kg body weight) in PBS containing 1% DMSO or vehicle was intraperitoneally injected into the mice 1 d before and 1, 3, 4, 5, and 6 d after SARS-CoV-2 infection, and body weight was measured. The humane endpoint was set at a 25% body weight loss relative to the initial body weight at the time of infection. The day that the mice had less than 75% body weight to the initial body weight was defined as the day of death. The animal experiments using SARS-CoV-2 were approved by the ethics committee of Osaka University (approval number BIKEN-AP- R02-09-0).

Preparation of Lung Tissues and RNAs from SARS-CoV2-Infected Mice. Male BALB/c mice (8 wk old) were intranasally injected with SARS-CoV-2 (MA10; 2×10^5 PFU/mouse). Four days after infection, the lungs were harvested. For the preparation of K02288-treated mice, K02288 (2 mg/kg body weight) in PBS containing 1% DMSO) or vehicle was intraperitoneally injected into the mice 1 d before and 1 and 3 d after SARS-CoV-2 infection. The lungs were harvested. The lungs were used for RNA preparation or fixed with 1 to 4% paraformaldehyde (PFA) and then used for the preparation of frozen sections.

Hematoxylin and Eosin Staining. The 4% PFA-fixed mouse lung sections were stained with hematoxylin and eosin Y (H&E, Fujifilm Wako Pure Chemical Corporation) and analyzed using the BZ-X700 (KEYENCE).

Ultrathin Section Transmission Electron Microscopy. The harvested mouse lungs were fixed in 0.1 M cacodylate buffer (pH7.4) containing 2% PFA and 2%

glutaraldehyde and subsequently post-fixed in 0.1 M cacodylate buffer containing 2% osmium tetroxide. After the fixation, the lungs were dehydrated in a graded series of ethanol and embedded in epoxy resin. Ultrathin sections were prepared, stained with 2% uranyl acetate and lead staining solution, and examined using an electron microscope (JEM-1400Plus; JEOL Ltd.) at 100 kV equipped with a CCD camera (EM-14830RUBY2; JEOL Ltd.).

Statistical Analysis. Data are expressed as mean \pm SEM. *P*-values were calculated using the log-rank test, unpaired *t* test, and one-way or two-way ANOVA followed by Tukey's test or Dunnett's test. All statistical analyses were performed using the Prism 7 software (GraphPad Software Inc.). The statistical significance of the differences in the means was determined using the tests indicated in the figure legends.

Study Approval. All animal experiments with or without SARS-CoV-2 were approved by the ethics committee of Osaka University (approval numbers: Douyaku-30-11-2 and BIKEN-AP-R02-09-0, respectively). All animal experiments were conducted in accordance with the guidelines of the Osaka University for the ethical treatment of animals. The experiments for SARS-CoV-2 isolation were approved by the research ethics committee of the Kyoto University (R2379-3).

Data, Materials, and Software Availability. All study data are included in the article and/or SI Appendix.

ACKNOWLEDGMENTS. We thank Ms. Shiori Manabe, Mr. Ryosuke Ishiba, Mr. Taito Kashio, and Mr. Kazuto Nunomura (Osaka University) for their technical assistance in library screening. We thank Dr. Miki Nagao and Dr. Yasufumi Matsumura (Kyoto University) for isolating SARS-CoV-2. This research was supported by JSPS KAKENHI (20H03382, 20K21481, and 22K19377), AMED (JP21fk0108432h0001, JP22ama121054, JP22ama121052, and JP22gm1610005h0002), the Takeda Science Foundation, Japan Research Foundation for Clinical Pharmacology, the Mochida Memorial Foundation for Medical and Pharmaceutical Research, and the Nippon Foundation-Osaka University Project for Infectious Disease Prevention.

Author affiliations: ^aGraduate School of Pharmaceutical Sciences, Osaka University, Osaka 565-0871, Japan; ^bResearch Institute for Microbial Diseases, Osaka University, Osaka 565-0871, Japan; ^cBIKEN Center for Innovative Vaccine Research and Development, The Research Foundation for Microbial Diseases of Osaka University, Osaka 565-0871, Japan; ^dCenter for iPS Cell Research and Application, Kyoto University, Kyoto 606-8507, Japan; ^eCenter for Infectious Disease Education and Research, Osaka University, Osaka 565-0871, Japan; ^fDepartment of Integrative Vascular Biology, Faculty of Medical Sciences, University of Fukui, Fukui 910-1193, Japan; and ^gDepartment of Anatomy, Keio University School of Medicine, Tokyo 160-8582, Japan

Author contributions: M.M., A.Y., N. Tokunoh, K.S., N.S., M.T., K. Tsujikawa, C.O., Y.M., N. Takakura, Y.K., K. Takayama, Y.Y., Y.F., and Y.O. designed research; M.M., A.Y., N. Tokunoh, T.M., K.S., M.K., R.H., N.S., J.T., M.T., S.T., M.I., C.O., Y.M., H.K., K.Takayama, Y.Y., and Y.O. performed research; M.M., A.Y., T.M., K.S., M.K., N.S., J.T., M.O., N.H., K. Tsujikawa, T.D., K. Takayama, Y.Y., Y.F., and Y.O. analyzed data; and M.M., N.Tokunoh., K.S., M.O., K.Takayama, Y.Y., Y.F., and Y.O. wrote the paper.

Competing interest statement: The authors declare competing interest. The authors have organizational affiliations to disclose. N. Tokunoh and Y.Y. were employed by the Research Foundation for Microbial Diseases at Osaka University.

1. E. Dejana, F. Orsenigo, M. G. Lampugnani, The role of adherens junctions and VE-cadherin in the control of vascular permeability. *J. Cell Sci.* **121**, 2115–2122 (2008).
2. C. Cerutti, A. J. Ridley, Endothelial cell-cell adhesion and signaling. *Exp. Cell Res.* **358**, 31–38 (2017).
3. M. Corada *et al.*, Vascular endothelial-cadherin is an important determinant of microvascular integrity in vivo. *Proc. Natl. Acad. Sci. U.S.A.* **96**, 9815–9820 (1999).
4. F. E. Nwariaku *et al.*, Tyrosine phosphorylation of vascular endothelial cadherin and the regulation of microvascular permeability. *Surgery* **132**, 180–185 (2002).
5. D. J. Angelini *et al.*, TNF- α increases tyrosine phosphorylation of vascular endothelial cadherin and opens the paracellular pathway through fyn activation in human lung endothelia. *Am. J. Physiol. Lung. Cell Mol. Physiol.* **291**, L1232–L1245 (2006).
6. J. Gavard, J. S. Gutkind, VEGF controls endothelial-cell permeability by promoting the beta-arrestin-dependent endocytosis of VE-cadherin. *Nat. Cell Biol.* **8**, 1223–1234 (2006).
7. A. Ashkenazi *et al.*, Protection against endotoxemic shock by a tumor necrosis factor receptor immunoadhesin. *Proc. Natl. Acad. Sci. U.S.A.* **88**, 10535–10539 (1991).
8. C. J. Walsh *et al.*, Monoclonal antibody to tumor necrosis factor alpha attenuates cardiopulmonary dysfunction in porcine gram-negative sepsis. *Arch. Surg.* **127**, 138–145 (1992).
9. K. J. Tracey *et al.*, Anti-cachectin/TNF monoclonal antibodies prevent septic shock during lethal bacteremia. *Nature* **330**, 662–664 (1987).
10. L. Huminiemi, M. Gorn, S. Suchting, R. Poulos, R. Bicknell, Magic roundabout is a new member of the roundabout receptor family that is endothelial specific and expressed at sites of active angiogenesis. *Genomics* **79**, 547–552 (2002).
11. K. W. Park *et al.*, Robo4 is a vascular-specific receptor that inhibits endothelial migration. *Dev. Biol.* **261**, 251–267 (2003).
12. K. Shirakura *et al.*, The Robo4-TRAF7 complex suppresses endothelial hyperpermeability in inflammation. *J. Cell Sci.* **132**, jcs220228 (2019).
13. N. R. London *et al.*, Targeting Robo4-dependent Slit signaling to survive the cytokine storm in sepsis and influenza. *Sci. Transl. Med.* **2**, 23ra19 (2010).
14. T. Kashio *et al.*, HDAC inhibitor, MS-275, increases vascular permeability by suppressing Robo4 expression in endothelial cells. *Tissue Barriers* **9**, 1911195 (2021).
15. H. Zhao *et al.*, Endothelial Robo4 suppresses breast cancer growth and metastasis through regulation of tumor angiogenesis. *Mol. Oncol.* **10**, 272–281 (2016).
16. A. W. Koch *et al.*, Robo4 maintains vessel integrity and inhibits angiogenesis by interacting with UNC5B. *Dev. Cell* **20**, 33–46 (2011).
17. C. A. Jones *et al.*, Robo4 stabilizes the vascular network by inhibiting pathologic angiogenesis and endothelial hyperpermeability. *Nat. Med.* **14**, 448–453 (2008).
18. T. E. Walshe *et al.*, TGF- β is required for vascular barrier function, endothelial survival and homeostasis of the adult microvasculature. *PLoS One* **4**, e5149 (2009).
19. T. Ota *et al.*, Targets of transcriptional regulation by two distinct type I receptors for transforming growth factor- β in human umbilical vein endothelial cells. *J. Cell Physiol.* **193**, 299–318 (2002).
20. M. J. Goumans *et al.*, Balancing the activation state of the endothelium via two distinct TGF- β type I receptors. *EMBO J.* **21**, 1743–1753 (2002).

21. L. David, C. Mallet, S. Mazerbourg, J. J. Feige, S. Bailly, Identification of BMP9 and BMP10 as functional activators of the orphan activin receptor-like kinase 1 (ALK1) in endothelial cells. *Blood* **109**, 1953–1961 (2007).
22. R. Hashimoto *et al.*, SARS-CoV-2 disrupts respiratory vascular barriers by suppressing Claudin-5 expression. *Sci. Adv.* **8**, eabo6783 (2022).
23. S. Suchting, P. Heal, K. Tahitis, L. M. Stewart, R. Bicknell, Soluble Robo4 receptor inhibits in vivo angiogenesis and endothelial cell migration. *FASEB J.* **19**, 121–123 (2005).
24. F. Zhang *et al.*, The Robo4 cytoplasmic domain is dispensable for vascular permeability and neovascularization. *Nat. Commun.* **7**, 13517 (2016).
25. M. J. Goumans *et al.*, Activin receptor-like kinase (ALK)1 is an antagonistic mediator of lateral TGFbeta/ALK5 signaling. *Mol. Cell* **12**, 817–828 (2003).
26. G. Deng, S. A. Curriden, S. Wang, S. Rosenberg, D. J. Loskutoff, Is plasminogen activator inhibitor-1 the molecular switch that governs urokinase receptor-mediated cell adhesion and release? *J. Cell Biol.* **134**, 1563–1571 (1996).
27. S. Lamouille, C. Mallet, J. J. Feige, S. Bailly, Activin receptor-like kinase 1 is implicated in the maturation phase of angiogenesis. *Blood* **100**, 4495–4501 (2002).
28. C. Mallet, D. Vittet, J. J. Feige, S. Bailly, TGFbeta1 induces vasculogenesis and inhibits angiogenic sprouting in an embryonic stem cell differentiation model: Respective contribution of ALK1 and ALK5. *Stem Cells* **24**, 2420–2427 (2006).
29. M. Scharpfenecker *et al.*, BMP-9 signals via ALK1 and inhibits bFGF-induced endothelial cell proliferation and VEGF-stimulated angiogenesis. *J. Cell Sci.* **120**, 964–972 (2007).
30. W. Li *et al.*, Circulating BMP9 protects the pulmonary endothelium during inflammation-induced lung injury in mice. *Am. J. Respir. Crit. Care Med.* **203**, 1419–1430 (2021).
31. Anonymous, Impact of selective anti-BMP9 treatment on tumor cells and tumor angiogenesis. *Mol. Oncol.* **10**, 1603–1620 (2016).
32. M. P. Panchenko, M. C. Williams, J. S. Brody, Q. Yu, Type I receptor serine-threonine kinase preferentially expressed in pulmonary blood vessels. *Am. J. Physiol.* **270**, L547–558 (1996).
33. E. S. Winkler *et al.*, SARS-CoV-2 causes lung infection without severe disease in human ACE2 knock-in mice. *J. Virol.* **96**, e0151121 (2022).
34. Y. Okada *et al.*, A three-kilobase fragment of the human Robo4 promoter directs cell type-specific expression in endothelium. *Circ. Res.* **100**, 1712–1722 (2007).
35. M. Hermann *et al.*, Binary recombinase systems for high-resolution conditional mutagenesis. *Nucleic Acids Res.* **42**, 3894–3907 (2014).
36. K. Okabe *et al.*, Neurons limit angiogenesis by titrating VEGF in retina. *Cell* **159**, 584–596 (2014).
37. S. Matsuyama *et al.*, Enhanced isolation of SARS-CoV-2 by TMPRSS2-expressing cells. *Proc. Natl. Acad. Sci. U.S.A.* **117**, 7001–7003 (2020).
38. S. Torii *et al.*, Establishment of a reverse genetics system for SARS-CoV-2 using circular polymerase extension reaction. *Cell Rep.* **35**, 109014 (2021).
39. S. R. Leist *et al.*, A mouse-adapted SARS-CoV-2 induces acute lung injury and mortality in standard laboratory mice. *Cell* **183**, 1070–1085.e1012 (2020).
40. S. Deguchi *et al.*, Usability of polydimethylsiloxane-based microfluidic devices in pharmaceutical research using human hepatocytes. *ACS Biomater. Sci. Eng.* **7**, 3648–3657 (2021).
41. E. Sano *et al.*, Cell response analysis in SARS-CoV-2 infected bronchial organoids. *Commun. Biol.* **5**, 516 (2022).